

Structural Studies and Cytotoxicity Assays of “Aggregation-Prone” IAPP_{8–16} and its Non-Amyloidogenic Variants Suggest its Important Role in Fibrillogenesis and Cytotoxicity of Human Amylin

Nikolaos N. Louros,¹ Paraskevi L. Tsiolaki,¹ Aikaterini A. Zompra,² Eleni V. Pappa,² Vassiliki Magafa,² George Pairas,² Paul Cordopatis,^{2†} Christina Cheimonidou,¹ Ioannis P. Trougakos,¹ Vassiliki A. Iconomidou,¹ Stavros J. Hamodrakas¹

¹Department of Cell Biology and Biophysics, Faculty of Biology, University of Athens, Panepistimiopolis, Athens 157 01, Greece

²Department of Pharmacy, University of Patras, Patras 26504, Greece

Received 26 December 2014; revised 10 March 2015; accepted 30 March 2015

Published online 25 April 2015 in Wiley Online Library (wileyonlinelibrary.com). DOI 10.1002/bip.22650

ABSTRACT:

Amyloid deposits to the islets of Langerhans are responsible for the gradual loss of pancreatic β -cells leading to type II diabetes mellitus. Human mature islet amyloid polypeptide (hIAPP), a 37-residue pancreatic hormone, has been identified as the primary component of amyloid fibrils forming these deposits. Several individual segments along the entire sequence length of hIAPP have been nominated as regions with increased amyloidogenic potential, such as regions 8–20, 20–29, and 30–37. A smaller fragment of the 8–20 region, spanning residues 8–16 of hIAPP has been associated with the formation of early transient α -helical dimers that promote fibrillogenesis and also as a core part of hIAPP amyloid fibrils. Utilizing our aggregation propensity prediction tools AmylPred and AmylPred2, we have identified the high aggregation propensity of the 8–16 segment of hIAPP. A peptide analog corresponding to this segment was chemically synthesized and its amyloidogenic properties were vali-

dated using electron microscopy, X-ray fiber diffraction, ATR FT-IR spectroscopy, and polarized microscopy. Additionally, two peptides introducing point mutations L12R and L12P, respectively, to the 8–16 segment, were chemically synthesized. Both mutations disrupt the α -helical properties of the 8–16 region and lower its amyloidogenic potential, which was confirmed experimentally. Finally, cytotoxicity assays indicate that the 8–16 segment of hIAPP shows enhanced cytotoxicity, which is relieved by the L12R mutation but not by the L12P mutation. Our results indicate that the chameleon properties and the high aggregation propensity of the 8–16 region may significantly contribute to the formation of amyloid fibrils and the overall cytotoxic effect of hIAPP. © 2015 Wiley Periodicals, Inc. *Biopolymers (Pept Sci)* 104: 196–205, 2015.

Keywords: islet amyloid polypeptide (IAPP); amylin; amyloid fibrils; peptide analogs; type II diabetes mellitus; cytotoxicity assays

[†]Deceased 10 October 2014.

Additional Supporting Information may be found in the online version of this article.

Correspondence to: Stavros J. Hamodrakas, Department of Cell Biology and Biophysics, Faculty of Biology, University of Athens, Panepistimiopolis, Athens 157 01, Greece; e-mail: shamodr@biol.uoa.gr

Disclosure: The authors declare no competing financial interests.

© 2015 Wiley Periodicals, Inc.

This article was originally published online as an accepted preprint. The “Published Online” date corresponds to the preprint version. You can request a copy of any preprints from the past two calendar years by emailing the *Biopolymers* editorial office at biopolymers@wiley.com.

INTRODUCTION

Human islet amyloid polypeptide (hIAPP), also known as amylin, is a 37 residue peptide hormone expressed and secreted along with insulin through the secretory granules of the pancreatic β -cells.¹ It is initially expressed as an 89 amino acid pre-hormone containing a 22-residue signal peptide and two flanking peptides (9-aa and 16-aa, respectively), both cleaved during secretion.^{2,3} Mature hIAPP has an amidated C-terminal end and contains an intramolecular disulfide bond formed between C₂ and C₇ residues⁴ (Figure 1). The physiological role of hIAPP is not fully understood yet, however its functions seem to be mediated by binding to specific receptors of the calcitonin related peptides (CTRs).^{5,6} Proposed functions briefly include promotion of satiety⁷⁻⁹ and suppression of adiposity,¹⁰ gastric emptying,¹¹ regulation of glucose homeostasis,^{12,13} and vasodilation.¹⁴

A growing number of proteins and peptides with unrelated functions and no apparent sequence similarity have been associated with the creation of amyloid fibrils via self-aggregation procedures.¹⁵⁻¹⁷ Deposition of amyloid fibrils in several tissues and organs has been identified as the main cause of a category

of diseases, known as amyloidoses,¹⁸ the so-called ‘conformational diseases’. Like several polypeptide hormones, which are over-represented as amyloid-forming proteins, hIAPP can be deposited as amyloid.¹⁹ Specifically, hIAPP has been recognized as the major component of pancreatic amyloid deposits which lead to gradual loss of β cells.^{20,21} Destruction of the β cells results in a decrease in production of insulin and IAPP causing type 2 diabetes (T2D).^{22,23}

Extensive biophysical and computational studies have indicated that short sequence fragments with high aggregation propensity may promote the amyloidogenic propensity of a protein.^{15,16} Numerous, extensive studies focused on ‘aggregation-prone’ segments have been performed in the case of hIAPP.²⁴⁻²⁸ Additional studies have implicated the 8–20 N-terminal region of IAPP with the formation of amyloid fibrils.^{29,30} These studies have also shown that fibrils formed by the aforementioned segment share several common characteristics to the fibrils formed by hIAPP. Later on, it was proposed that this region may be driven by the self-aggregating 15–20 segment.²⁸ Here by implementing our algorithms AmylPred and AmylPred 2 (Supporting Information Figure S1) on the sequence of hIAPP (see ‘Materials and Methods’ section and

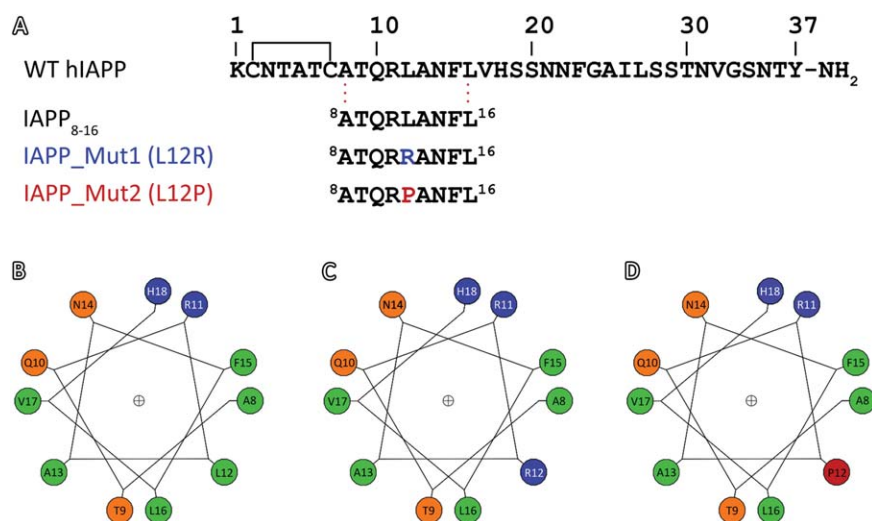


FIGURE 1 The amphipathic properties of the 8–16 α -helical segment of hIAPP. (A) A peptide analog IAPP₈₋₁₆ (ATQLANFL) was synthesized in order to study the aggregation properties of the 8–16 helical segment of hIAPP. Two additional peptides, containing point mutations: IAPP_Mut1 (L12R, shown in blue) and IAPP_Mut2 (L12P, shown in red) were also synthesized. (B) Helical wheel representation of the amphipathic 8–16 α -helical segment of hIAPP. The hydrophobic interface formed by residues A8, L12, F15, and L16 has been proposed to be important for early oligomerization of IAPP³¹. (C) Introduction of the L12R mutation disrupts the hydrophobic cluster and therefore might hinder the formation of early oligomers leading to amyloid fibril formation. (D) The L12P mutation introduces a kink in the central L12 position of the 8–16 α -helix, altering its structural integrity and polymerization potential. Aliphatic residues are shown as green circles, polar residues are shown as orange circles, positively charged residues are shown as blue circles and proline residues are shown as red circles, respectively. Helical wheels were constructed using the Helical Wheel program developed by Dr. Kael Fischer (<http://kael.net/helical.htm>).

Supporting Information), we identified and experimentally studied the aggregation propensity of the 8–16 segment of hIAPP, which has also been associated with the formation of early oligomerization events of IAPP.³¹ Our experimental results presented here, clearly show that the 8–16 segment of hIAPP self-assembles forming fibrils with amyloid properties similar to full length hIAPP and therefore verify the high amyloidogenic potential of this region, but may also imply that the 8–16 segment might actually be one of the stronger self-aggregating motifs that lead hIAPP to polymerization. Furthermore, two peptide analogs corresponding to variants of the same segment were also synthesized, introducing point mutations of the central L12 residue to R and P residues, respectively. Both peptides were experimentally tested and were found to have a significantly lower amyloidogenic propensity, since they do not form amyloid fibrils. Finally, cytotoxic assays performed for all three peptide analogs indicate that the peptide analog corresponding to the 8–16 segment of hIAPP has enhanced cell cytotoxicity. Interestingly, the peptide analog containing the L12P mutation also exhibits cytotoxicity regardless of its lowered amyloidogenic propensity, whereas the second variant containing the L12R mutation has no cytotoxic effects. These results indicate that the 8–16 segment of hIAPP may contribute in the overall toxicity of the molecule and therefore is an essential target for the development of inhibitory agents or novel treatments against T2D.

MATERIALS AND METHODS

Prediction of IAPP “Aggregation-Prone” Segments and its Nonamyloidogenic Variants

In order to successfully identify segments of human mature IAPP presenting a high aggregation tendency, we applied AmylPred and AmylPred2, two aggregation propensity consensus prediction tools, combining 5 and 11 individual algorithms, respectively, which were developed by our laboratory^{15,32} on the sequence of IAPP (Supporting Information Figure S1). As a result, a segment corresponding to residues 8–16 of hIAPP was identified with high aggregation propensity. Theoretical and experimental evidence reveal that this segment is also part of an α -helical segment following the C₂–C₇ disulphide bridge (Figure 1B).^{31,33–35} For this reason, we introduced two individual point mutations, L12R and L12P which lower the aggregation potency of the aforementioned area and significantly alter its structural integrity (Figures 1C and 1D). Both mutant peptides were also predicted to have a diminished self-polymerizing potential, compared to the native peptide (Supporting Information Figure S1).

Peptide Synthesis and Preparation of Amyloid-like Fibrils

To experimentally investigate the aggregation potential of the 8–16 segment, a peptide analog, ⁸ATQRLANFL¹⁶ (IAPP_{8–16}) was chemically

synthesized (Figure 1A). To further validate the calculated reduction in amyloidogenicity introduced by the L12R and L12P mutations, two additional peptide analogs were also synthesized, ⁸ATQRRANFL¹⁶ (IAPP_Mut1), and ⁸ATQRPANFL¹⁶ (IAPP_Mut2), respectively (Figure 1A). The peptides were synthesized by the solid phase methodology and Fmoc/^tBu chemistry, using 2-chlorotrityl chloride resin as a solid support.³⁶ The final products were determined to be at least 97% pure by analytical HPLC. Solutions of all three peptides were prepared in distilled water (pH 5.75) at a final concentration of 10 mg/ml, following previous structural studies of aggregation-prone peptides with amyloidogenic properties.^{25,26,29,37–40} After an incubation period of 7 days at ambient temperature, the IAPP_{8–16} peptide produced gels containing mature amyloid-like fibrils, as judged by electron microscopy (EM) studies (see below). In contrast, both mutant peptides did not produce amyloid fibrils even after a period of up to 8 months.

Transmission Electron Microscopy (Negative Staining)

Drops (~5 μ l) of all three peptide solutions were applied to 400-mesh glow-discharged and carbon-coated copper grids for 60–80 s. The grids were stained with a drop of 2% (w/v) aqueous uranyl acetate for 60 s. Excess stain was removed by blotting with a filter paper. The grids were initially air-dried and examined with a MorgagniTM 268 transmission electron microscope, operated at 80 kV. Digital acquisitions were performed with an 11 Mpixel side-mounted Morada CCD camera (Soft Imaging System, Muenster, Germany).

Congo Red Staining and Polarized Light Microscopy

Films were formed by applying drops of each peptide solution to glass slides and subsequently air-dried at ambient temperatures and humidity. The films were then stained with a 1% Congo red solution in distilled water (pH 5.75) for 20 min, following the typical Romhanyi protocol,⁴¹ as previously shown.^{37,39} Excess stain was removed through tap water washes.⁴¹ Samples were observed under bright field illumination and between crossed polars, using a Leica MZ75 polarizing stereomicroscope equipped with a JVC GC-X3E camera.

X-Ray Fiber Diffraction

Droplets (10 μ l) of the peptide solutions were placed between two aligned capillaries with wax-covered ends (spaced 2 mm apart). The droplets were allowed to dry slowly at ambient temperature and humidity, for 30–60 min in order to form an oriented fiber suitable for X-ray diffraction. X-ray diffraction patterns were collected, using a SuperNova-Agilent Technologies X-ray generator equipped with a 135-mm ATLAS CCD detector and a 4-circle kappa goniometer, at the Institute of Biology, Medicinal Chemistry and Biotechnology, National Hellenic Research Foundation (CuK _{α} high intensity X-ray micro-focus source, $\lambda = 1.5418 \text{ \AA}$), operated at 50 kV, 0.8 mA. The specimen-to-film distance was set at 52 mm. The exposure time was set to 360 s. The X-ray diffraction patterns were initially viewed using the program CrysAlisPro⁴² and subsequently displayed and measured with the aid of the program iMosFLM.⁴³

Attenuated Total Reflectance Fourier-Transform Infrared Spectroscopy and Postrun Spectra Computations

Suspensions ($\sim 5 \mu\text{l}$) of the peptide solutions were cast on flat stainless-steel plates coated with an ultrathin hydrophobic layer (Spec-TRIM, Tienta Sciences, Indianapolis, USA) and left to dry slowly at ambient conditions to form thin films. IR spectra were obtained at a resolution of 4 cm^{-1} , utilizing an IR microscope (IRScope II, Bruker-OPTICS, Bruker Optik GmbH, Ettlingen, Germany), equipped with a Ge ATR objective lens (20 \times) and attached to a FT-IR spectrometer (Equinox 55, BrukerOPTICS). Ten 32-scan spectra were collected from each sample and averaged to improve the S/N ratio. Spectra are shown in the absorption mode, after correction for the wavelength dependence of the penetration depth (d_p analogs λ). Derivatives were computed analytically using routines of the Bruker OPUS/OS2 software including smoothing over a $\pm 8 \text{ cm}^{-1}$ range around each data point, performed by the Savitsky–Golay algorithm.⁴⁴ Smoothing over narrower ranges resulted in deterioration of the S/N ratio and did not increase the number of minima that could be determined with confidence. The minima in the second derivative were used to determine the corresponding absorption band maxima.

Cytotoxicity Assays

Human PANC-1 cells (derived from a patient with epithelioid carcinoma in the pancreatic duct) were plated in 96-well plates at a density of 5×10^3 cells/well. Cells were incubated for 24 h in Dulbecco's Modified Eagle's Medium (DMEM) supplemented with 10% fetal bovine serum (FBS) at 37° in 5% CO₂. Stock solutions of peptides IAPP_{8–16}, IAPP_Mut1, and IAPP_Mut2 were prepared in ddH₂O at a concentration of 10 mg/ml, similarly to the biophysical studies in order to keep track of the aggregation propensity of each peptide. Peptide toxicity was assessed after 1, 3, 15, and 30 days of incubation, respectively. The final concentration of peptides in the culture medium was set to 200 μM , based on similar previous cytotoxicity studies of IAPP fragment peptides.^{26,30,45–47} The MTT dye (1 mg/ml in phenol red free DMEM w/o FBS) was added 24 h after the addition of the peptides. Reduction of the dye by living cells was allowed to take place for 3–4 h. The MTT solution was discarded and isopropanol was added to dissolve the formazan crystals. Absorbance of the solution was measured at 570 nm wavelength. Survival of nontreated cells was set to 100%.

RESULTS

EM studies reveal that the IAPP_{8–16} peptide self-assembles forming ordered elongated fibrils, which appear unbranched and straight, with a tendency to wrap around each other forming twisted cords, approximately 100–120 Å in diameter (Figure 2A, arrows). In contrast, the IAPP_Mut1 peptide analog did not produce amyloid-like fibrils under the same conditions, even for longer incubation periods up to 8 months. Instead, the IAPP_Mut1 peptide forms small spherical aggregates or thin worm-like shaped aggregates that closely resemble prefibrillar aggregates as has been shown for other amyloidogenic proteins (Figure 2B).⁴⁸ The IAPP_Mut2 peptide did not produce

amyloid fibrils at similar conditions, as has theoretically been predicted. However, unlike the IAPP_Mut1 mutant peptide, in this case, only amorphous aggregates were formed (Figure 2C), indicating that the insertion of a proline residue might reduce the high amyloidogenic potential of the 8–16 segment of IAPP in a more drastic manner. Incubation for longer time periods up to 8 months did not result in any changes in the morphology of the aggregates formed by both the IAPP_Mut1 and IAPP_Mut2 peptides (see “Materials and Methods”).

The X-ray diffraction pattern produced from an oriented fiber containing aligned amyloid-like fibrils derived by self-assembly of the IAPP_{8–16} “aggregation-prone” peptide indicated that the fibrils adopt the typical for amyloids “cross- β ” structure (Figure 3). Specifically, the diffraction pattern presents a strong 4.7 Å reflection along the meridian axis (fibril axis), corresponding to the repetitive distance between perpendicularly to the axis of the fiber aligned, hydrogen bonded, β -strands and a 10.1 Å equatorial reflection that might be attributed to the packing distance of formed β -sheets. Both mutant peptide analogs, however, did not produce fibers under the same conditions, in agreement to the results of our EM studies, which suggest their inability to form amyloid fibrils.

Supporting evidence regarding the secondary structure of the IAPP_{8–16} peptide forming amyloid-like fibrils was obtained utilizing ATR FT-IR spectroscopy. The ATR FT-IR spectrum derived from a thin hydrated film containing amyloid-like fibrils from the IAPP_{8–16} peptide, strongly suggests that the peptide adopts an antiparallel β -sheet conformation, in agreement to the X-ray diffraction results (Figure 4). The spectrum contains a prominent 1622 cm^{-1} amide I band, accompanied by a 1539 cm^{-1} amide II band, both indicating the preponderance of a β -sheet secondary structure.^{49–52} The 1697 cm^{-1} shoulder most probably indicates that the β -strands are aligned in an antiparallel fashion (Table I).⁵³

Amyloid-like fibril samples have been shown to specifically bind the Congo red dye, showing the characteristic for amyloids red-green/apple birefringence, in a polarizing microscope under crossed polars.⁵⁴ Therefore, similar staining procedures were carried out for all three peptides: Clearly, films formed by the amyloid-like fibril containing solutions of the IAPP_{8–16} peptide (see Materials and Methods) bind the Congo red dye, as seen under bright field illumination and furthermore exhibit the characteristic apple/green birefringence of amyloids (Figure 5). Interestingly, multiple and variable in size spherical structures, known as spherulites are present in the solutions. These structures have a liquid crystalline texture and present characteristic “Maltese crosses”^{55,56} (Figure 5, arrows). In contrast, similar experiments that were performed for the two mutant peptides, IAPP_Mut1 and IAPP_Mut2 indicated their inability to bind the Congo red dye.

The cytotoxic effect of hIAPP fibrils on pancreatic cell lines has been extensively documented.^{57–59} Here, we investigated whether the 8–16 region of hIAPP may contribute to the cyto-

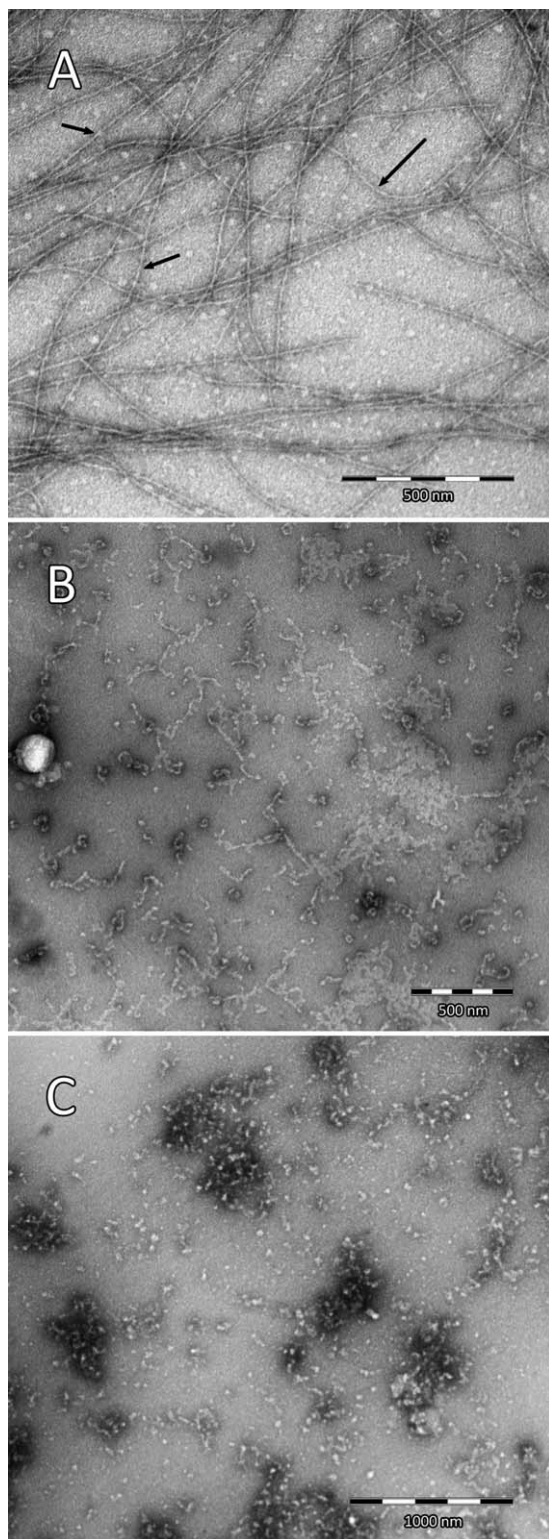


FIGURE 2.

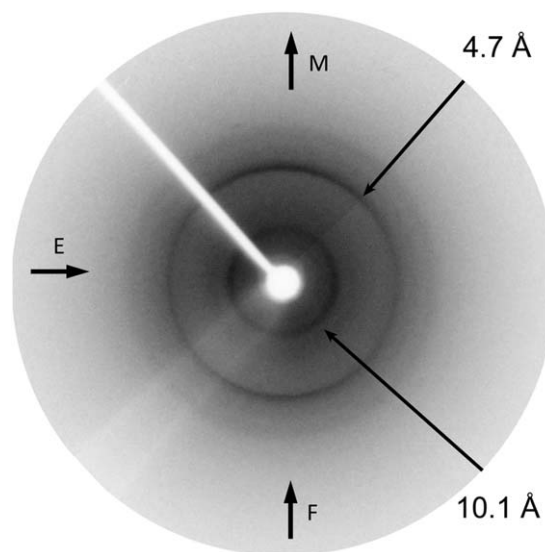


FIGURE 3 X-ray fiber diffraction pattern produced by an aligned fiber containing IAPP_{8–16} amyloid-like fibrils. A typical “cross- β ” diffraction pattern is shown from oriented fibers, derived from IAPP_{8–16} amyloid-like fibrils. The strong 4.7 Å meridional reflection (*M*) corresponds to the repeat distance of β -strands aligned perpendicularly to the fiber axis (*F*), whereas the 10.1 Å equatorial (*E*) reflection is attributed to the packing distance between β -sheets.

toxicity of the full length molecule by examining the cytotoxicity of the IAPP_{8–16} peptide, and, additionally, if the non-amyloidogenic mutants IAPP_Mut1 and IAPP_Mut2 present similar cytotoxic effects. Each peptide was added in PANC-1 cells after an incubation period of 1, 3, 15, and 30 days respectively, in order to assess the toxicity of the peptides at early and late stages of fibrillogenesis. Our results clearly indicate that the IAPP_{8–16} peptide induces a cytotoxic effect ($\sim 76\%$ cell survival in relation to the control) after 1 day of incubation

FIGURE 2 Electron microscopy studies of the aggregation propensity of IAPP_{8–16}, IAPP_Mut1 and IAPP_Mut2 peptide analogs. (A) Electron micrograph of amyloid-like fibrils formed by the self-aggregating IAPP_{8–16} peptide (10 mg/mL) following incubation for a period of 7 days. The fibrils are long and unconnected with a double helical morphology and a diameter of approximately 100–120 Å. Scale bar 200 nm. (B) Electron micrograph indicating the inability of the IAPP_Mut1 peptide to form amyloid-like fibrils, under similar conditions. After incubation for 1 week the peptide forms small spherically shaped or worm-like aggregates possibly resembling the morphology of prefibrillar aggregates.⁴⁸ However, incubation for longer periods (up to 8 months) did not result to any difference in morphology (data not shown). Scale bar 500 nm. (C) Electron micrograph indicating that the IAPP_Mut2 peptide does not form amyloid-like fibrils at the same conditions. Amorphous aggregates are formed, even after incubation for longer periods (up to 8 months) suggesting that the L12P mutation strongly inhibits the aggregation propensity of the 8–16 segment. Scale bar 1000 nm.

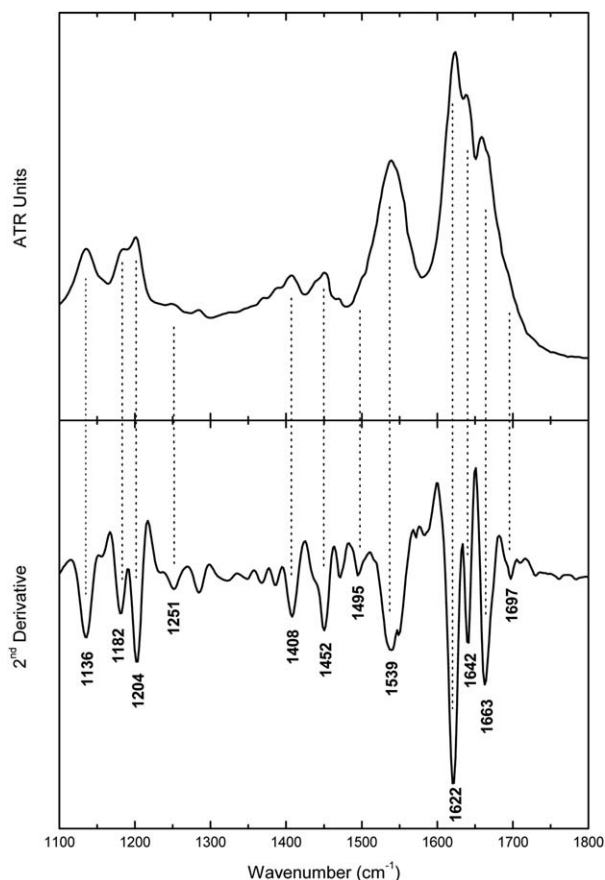


FIGURE 4 ATR FT-IR spectrum (1100–1800 cm^{-1}) obtained from a thin hydrated film containing IAPP_{8–16} amyloid-like fibrils. The derived spectrum indicates that the amyloid-like fibrils adopt an antiparallel β -sheet secondary structure. Identification of the band maxima and their tentative assignments was performed utilizing second derivative spectral analysis (Table I).

(Figure 6A) and more or less similar cytotoxicity after 3 (Figure 6B) and 30 days (Figure 6D) of incubation (~ 74 and 83% cell survival). Results obtained after 15 days of incubation (Figure 6C) indicate a slightly lower cytotoxicity ($\sim 92\%$ cell survival), however these results also exhibit an unusually large standard deviation in comparison to the rest, implying that the cytotoxic effect might actually be higher than that observed. These data suggest that the amyloidogenicity presented by the 8–16 region of hIAPP may play a vital role in the cytotoxic effect of the full length molecule.

Similar experiments indicate no significant cytotoxicity for the IAPP_Mut1 peptide (Figure 6). This apparently suggests that the L12R mutation that was found to inhibit fibrillogenesis, may also significantly lower the toxicity presented by the 8–16 region of hIAPP. In contrast, although the IAPP_Mut2 peptide did not exhibit any amyloidogenic properties, it does display enhanced cell toxicity, since it was found to be toxic after incubation for 1, 3, 15, and 30 days (~ 70 , 79, 72, and

Table I Bands Observed in the ATR FT-IR Spectrum Produced from a Hydrated Film of the ‘Aggregation-Prone’ IAPP_{8–16} Peptide, After Self-Assembly, and their Tentative Assignments (Figure 4)

Bands (cm^{-1})	Assignment
1136	TFA
1182	TFA
1204	TFA
1251	β -sheet (amide III)
1452	CH_2 deformation
1499	Phe
1539	β -sheet (amide II)
1622	β -sheet (amide I)
1642	β -sheet (amide I)
1663	TFA
1697	Antiparallel β -sheet

$\sim 89\%$ cell viability, respectively) (Figure 6). This finding suggests that the IAPP_Mut2 peptide is toxic to PANC-1 cells for unknown reasons, obviously not related to fibrillogenesis.

DISCUSSION

Several theoretical and experimental studies have focused on the amyloidogenic properties of short sequence fragments of amyloid-forming proteins indicating that specific regions are responsible for the fibrillogenetic potential of the full length protein.^{15,16} Our results indicate that the IAPP_{8–16} peptide analog self-assembles forming fibrils with an amyloid-like morphology, typical “cross- β ” architecture and the ability to bind the specific for amyloids Congo red dye. Importantly, EM studies performed by our lab on hIAPP indicate that amyloid fibrils with a comparable similarity to the IAPP_{8–16} fibrils are formed, since they frequently appear as straight and unconnected double helices, with a diameter of 100–120 Å and an indeterminate length (Supporting Information Figure S2A). These results are further supported by previous elaborate EM studies indicating that hIAPP leads to the formation of mature amyloid fibrils composed of supercoiled protofilaments with a 10 nm diameter.^{60–62} Furthermore, the X-ray diffraction pattern produced by an oriented fiber containing more or less aligned hIAPP amyloid fibrils (Supporting Information Figure S2B) is comparable to the one produced by the IAPP_{8–16} peptide, with a 4.7 Å meridian and a 10.1 Å equatorial reflection, respectively, as also previously shown,²⁹ indicating possible similarities in the “cross- β ” structure of amyloid fibrils formed in both cases. The above suggest that IAPP_{8–16} probably has a central role in the IAPP fibrillogenesis process.

hIAPP fibrillogenesis has been stated to be a multistage progressive process, beginning with the formation of initial

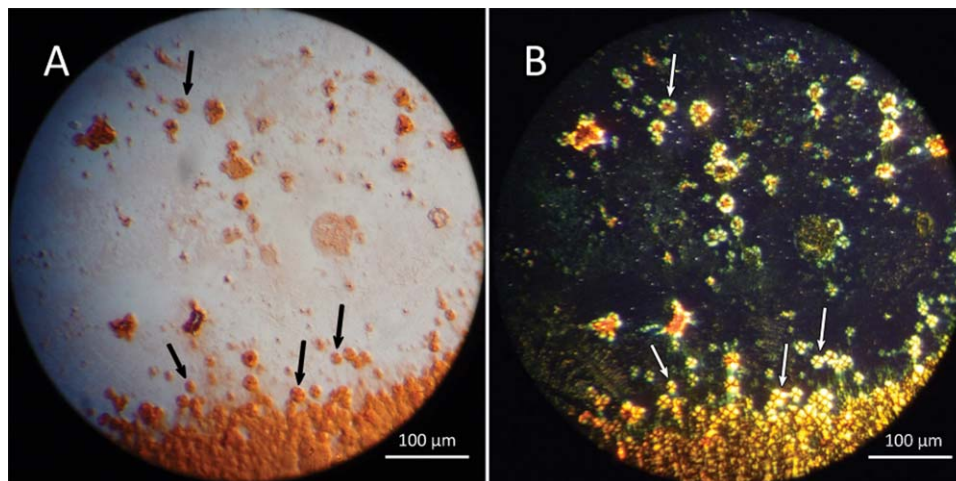


FIGURE 5 Dehydrated films derived from drops of the IAPP_{8–16} solution display Congo red birefringence, characteristic of amyloid fibrils. (A) Gels containing IAPP_{8–16} amyloid-like fibrils are positively stained with the Congo red dye, as seen under bright field illumination. Spherical aggregates known as spherulites are formed, which also successfully bind the Congo red dye (arrows). (B) Under crossed polars, a yellow to apple/green birefringence, characteristic of amyloids, is evident. Furthermore, the typical “Maltese crosses” of the spherulites are also viewed (arrows). Scale bars 100 μm .

metastable intermediates that develop to protofibrils which eventually give rise to the mature hIAPP amyloid fibrils.⁶¹ Our results also showed that IAPP_{8–16} amyloid fibril formation is a nucleation dependent process, since the peptide forms spherulites (Figure 5, arrows). These liquid crystalline spherical structures are ordered arrays of fibrils and have been nominated as prefibrillar species, probably cytotoxic, which are formed in early amyloidogenesis events of proteins associated both with functional⁵⁵ and pathological amyloids.^{38,56} Interestingly, impressive work by Fraser and co-workers has shown that proIAPP^{1–48} polymerizes forming amyloid fibrils, initially forming spherulites with typical Maltese crosses.⁶³ Therefore, the ability of the IAPP_{8–16} peptide to form spherulites indicates that this segment might contribute vitally in the early fibrillogenesis events of hIAPP.

Regarding the molecular mechanism of hIAPP aggregation, several models have been proposed previously. Early studies indicated that the 8–20 region may benefit hIAPP oligomerization into a triple β -stranded structure, in cooperation with the 20–29 and 30–37 segments.²⁹ A detailed model of the structure of hIAPP protofilaments was derived through solid-state NMR studies, which was also in agreement with STEM and AFM results presenting hIAPP protofilament morphologies.⁶⁴ This model proposes that hIAPP is folded in a β -hairpin structure with the β -strands formed by residues 8–17 (strongly overlapping the IAPP_{8–16} peptide) and 27–37.^{35,64} Concomitant evidence utilizing two-dimensional IR spectroscopy was obtained by Shim et al. verifying the aforementioned model.⁶⁵

Consequently, our results are in agreement with these models indicating a central role for the 8–16 fragment of hIAPP in the formation of amyloid fibrils, by elucidating the self-aggregation potency of the IAPP_{8–16} peptide analog.

Impressive evidence demonstrated that hIAPP dimer formation is an important step in the polymerization process.³¹ Specifically, it was shown that the 5–16 region of hIAPP, strongly overlapping the IAPP_{8–16} peptide of our study, has a high tendency to form dimers through α -helix- α -helix association,^{66,67} as previous NMR studies have also indicated.⁶⁸ This tendency was attributed to the presence of the L12, F15, and L16 residues that shape a hydrophobic interface which leads to the formation of α -helical dimers through intermolecular interactions.³¹ The same study proposed that these helical dimers play a vital role in the polymerization process of hIAPP, by acting as the early oligomers promoting the transition to the final amyloid “cross- β ” structure. A logical outcome of the above, dictates that destabilization of the α -helical dimer formation process could equally lead to destabilization of the amyloid fibril formation process. The L12 residue was shown to play a central role in dimerization through L12–F15 and L12–L16 hydrophobic interactions,³¹ therefore we attempted to test this assumption by introducing a charge at this site with the L12R mutation of the IAPP_Mut1 peptide (Figure 1C). Interestingly, our experimental results indicated that this mutation was sufficient enough to alleviate the aggregation propensity of the 8–16 hIAPP segment (Figure 2B). Furthermore, the L12P mutation, introducing a kink that would destabilize the

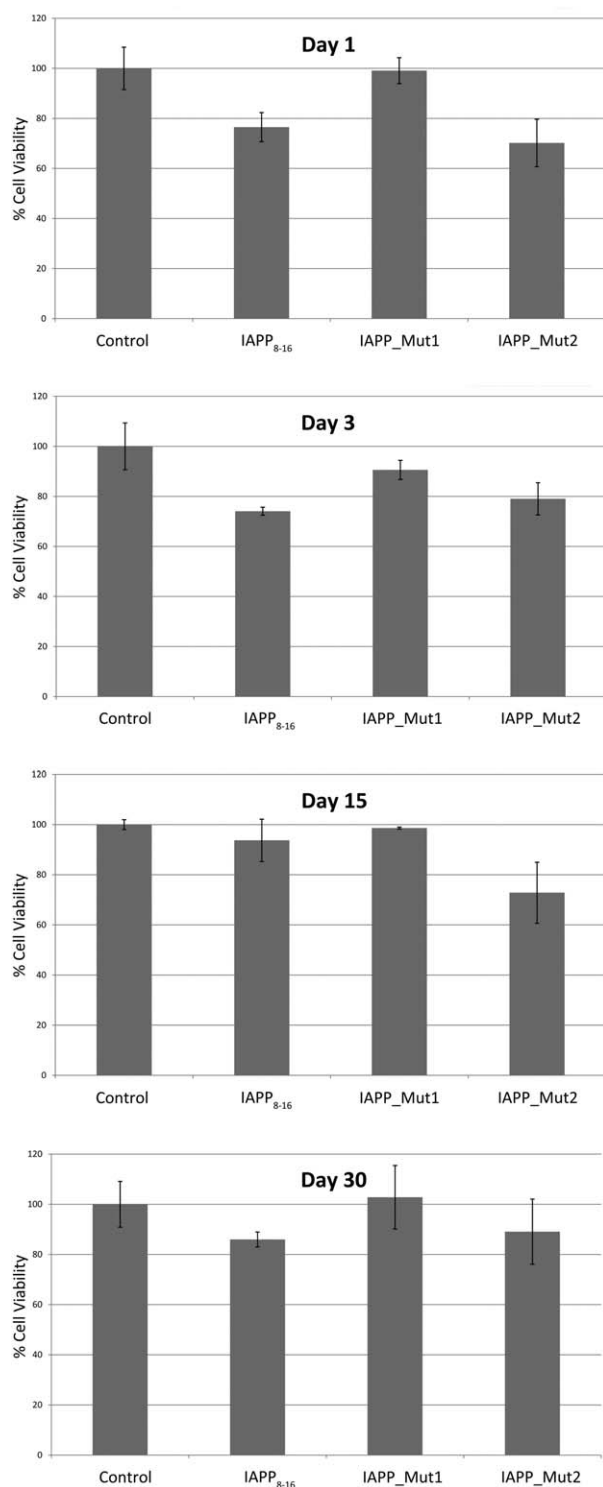


FIGURE 6 Cytotoxicity assays of peptides IAPP₈₋₁₆, IAPP_Mut1 and IAPP_Mut2 after incubation for (A) 1, (B) 3, (C) 15, and (D) 30 days, respectively. Results indicate that the IAPP₈₋₁₆ peptide has enhanced cytotoxicity even after 1 day of incubation. Comparably, although the IAPP_Mut2 peptide did not exhibit any amyloidogenic properties, it also exhibits significant cytotoxicity for unknown reasons. In contrast, the IAPP_Mut1 peptide did not exhibit any cytotoxicity even after 30 days of incubation.

early formed α -helical segment (Figure 1D), seemed to completely impede the self-aggregation process of the IAPP_Mut2 peptide, respectively (Figure 2C).

Extensive studies have previously indicated that hIAPP can induce a cytotoxic effect by forming either on-pathway amyloid fibrils that mechanically cause membrane fragmentation or by forming off-pathway intermediates that eventually lead to membrane disruption.⁶⁹⁻⁷² Several agents have been associated with this complicated process, such as zinc and calcium cations or insulin.⁷³⁻⁷⁷ Additional studies have shown that the 20-29 segment^{78,79} and the N-terminal 1-19 segment of hIAPP may play a crucial role in the cytotoxic effect of hIAPP.⁸⁰⁻⁸² NMR studies have reported the three-dimensional structures of both human and rat IAPP₁₋₁₉ (hIAPP₁₋₁₉ and rIAPP₁₋₁₉, respectively).⁸² Although hIAPP₁₋₁₉ differs in only one residue to rIAPP (H18R), it is significantly more toxic.⁸¹ These studies indicate that the observed difference is attributed to the presence of an extra positive charge in rIAPP that leads the peptide to adopt a nontoxic orientation, since it is bound to the membrane surface, in contrast to hIAPP which is inserted into the membrane, possibly in an oligomeric state, causing disruption.^{81,83,84} In agreement to the above, our results indicate that the 8-16 segment (core segment of the hIAPP₁₋₁₉ peptide) also has a severe cytotoxic effect. However, since the toxic levels of the peptide are not dependent on the incubation period (Figure 6), it seems possible that the toxicity may be attributed both to the formation of off-pathway oligomers at early stages and to mechanical disruption caused by amyloid fibril formation at late stages, due to its high aggregation propensity. The insertion of a positively charged residue in the case of the IAPP_Mut1 peptide completely diminished the cytotoxic effects of the 8-16 segment. However, since the additional charged residue concurrently lowered the aggregation potency of the segment, it is not clear whether the reduced toxicity is a result of inhibition of the fibrillogenesis process or the formation of toxic off-pathway intermediates, such as in the case of rIAPP₁₋₁₉. Finally, the results obtained in the case of the IAPP_Mut2 peptide indicate that the cytotoxic effect of the peptide remains although fibrillogenesis is diminished. These results imply that the toxicity of the 8-16 segment of hIAPP may not be a result of the formation of amyloid fibrils but instead relies to off-pathway events. Further experiments need to be performed in order to elucidate the role of the 8-16 segment in the toxicity of hIAPP, however, it seems that this segment vitally contributes in the cell toxicity of the full length molecule at any case.

Conclusively, our results reveal that the IAPP₈₋₁₆ fragment forms fibrils with similar amyloidogenic properties to hIAPP. Additionally, we showed that mutations which destabilize the

chameleon conformational properties of this segment and concurrently lower its aggregation propensity significantly hinder the amyloid fibril formation process. Our cytotoxicity experiments clearly showed that the 8–16 segment of hIAPP exhibits enhanced cytotoxicity and could therefore importantly contribute to the cytotoxic effect of the full length molecule (Supporting Information Figure S3). The L12R mutation diminished the amyloidogenic properties of the 8–16 segment and concurrently alleviated the cytotoxic properties exhibited by the same segment, whereas the L12P mutation did not, for unknown reasons. Summarizing, our results reveal that the IAPP_{8–16} fragment may significantly contribute both in the overall aggregation propensity and cytotoxicity of hIAPP. Combining previous results indicating that the same segment shows a prominent binding affinity for hIAPP,²⁸ it appears that this part of the molecule is of great interest since it may actually be an effective target for drug designing studies or other targeted remedies that will help in preventing hIAPP amyloid deposition or cytotoxicity and therefore help treat or inhibit the progression of T2D.

We should like to thank Dr. Evangelia Chrysinia for help with the X-ray experiments and the Institute of Biology, Medicinal Chemistry and Biotechnology, National Hellenic Research Foundation for allowing us to use the X-ray protein crystallography facility. The help of Dr. George Baltatzis and Prof. Efstratios Patsouris and the use of the Morgagni Microscope at the 1st Department of Pathology, Medical School, University of Athens are also gratefully acknowledged. We also thank the University of Athens for support. The authors sincerely thank the Editor in Chief and the Managing Editor for properly handling this manuscript and the anonymous reviewers for their very useful and constructive criticism, which helped us to considerably improve the manuscript. This research has been co-financed by the European Union (European Regional Development Fund–ERDF) and Greek national funds through the Operational Program “Competitiveness and Entrepreneurship” of the National Strategic Reference Framework (NSRF) (Project Code 11SYN-1–1230). We should like to devote this manuscript, in memory of our great friend and collaborator Prof. Paul Cordopatis, a Master in the field of Peptide Science, recently deceased.

REFERENCES

- Sanke, T.; Bell, G. I.; Sample, C.; Rubenstein, A. H.; Steiner, D. *F. J Biol Chem* 1988, 263, 17243–17246.
- Betsholtz, C.; Svensson, V.; Rorsman, F.; Engstrom, U.; Westermark, G.T.; Wilander, E.; Johnson, K.; Westermark, P. *Exp Cell Res* 1989, 183, 484–493.
- Mosselman, S.; Hoppener, J.W.; Lips, C.J.; Jansz, H.S. *FEBS Lett* 1989, 247, 154–158.
- Westermark, P.; Andersson, A.; Westermark, G. T. *Physiol Rev* 2011, 91, 795–826.
- McLatchie, L. M.; Fraser, N. J.; Main, M. J.; Wise, A.; Brown, J.; Thompson, N.; Solari, R.; Lee, M. G.; Foord, S. M. *Nature* 1998, 393, 333–339.
- Muff, R.; Buhlmann, N.; Fischer, J. A.; Born, W. *Endocrinology* 1999, 140, 2924–2927.
- Lutz, T. A. *Diabetes Obes Metab* 2012, 15, 99–111.
- Reidelberger, R. D.; Haver, A. C.; Arnelo, U.; Smith, D. D.; Schaffert, C. S.; Permert, J. *Am. J. Physiol. Regul. Integr. Comp Physiol* 2004, 287, R568–574.
- Potes, C. S.; Lutz, T. A. *Physiol Behav* 2010, 100, 511–518.
- Lutz, T. A. *Handb. Exp Pharmacol* 2012, 231–250.
- Kong, M. F.; King, P.; Macdonald, I. A.; Stubbs, T. A.; Perkins, A. C.; Blackshaw, P. E.; Moyses, C.; Tattersall, R. B. *Diabetologia* 1997, 40, 82–88.
- Lutz, T. A. *Am. J. Physiol Regul Integr Comp Physiol* 2010, 298, R1475–R1484.
- Lutz, T. A. *Cell. Mol. Life Sci* 2011, 69, 1947–1965.
- Abedini, A.; Schmidt, A. M. *FEBS Lett* 2013, 587, 1119–1127.
- Frousios, K. K.; Iconomidou, V. A.; Karletidi, C. M.; Hamodrakas, S. J. *BMC Struct Biol* 2009, 9, 44.
- Lopez de la Paz, M.; Serrano, L. *Proc Natl Acad Sci USA* 2004, 101, 87–92.
- Valery, C.; Pandey, R.; Gerrard, J. A. *Chem Commun* 2013, 49, 2825–2827.
- Sipe, J. D.; Benson, M. D.; Buxbaum, J. N.; Ikeda, S.; Merlini, G.; Saraiva, M. J.; Westermark, P. *Amyloid* 2012, 19, 167–170.
- Clark, A.; Cooper, G. J.; Lewis, C. E.; Morris, J. F.; Willis, A. C.; Reid, K. B.; Turner, R. C. *Lancet* 1987, 2, 231–234.
- Rocken, C.; Linke, R. P.; Saeger, W. *Virchows Arch. A Pathol Anat Histopathol* 1992, 421, 339–344.
- Westermark, P.; Wilander, E.; Westermark, G. T.; Johnson, K. H. *Diabetologia* 1987, 30, 887–892.
- Schneider, H. M.; Storkel, S.; Will, W. *Dtsch Med Wochenschr* 1980, 105, 1143–1147.
- Westermark, P.; Johnson, K. H. *BioEssays* 1988, 9, 30–33.
- Westermark, P.; Engstrom, U.; Johnson, K. H.; Westermark, G. T.; Betsholtz, C. *Proc Natl Acad Sci USA* 1990, 87, 5036–5040.
- Nilsson, M. R.; Raleigh, D. P. *J Mol Biol* 1999, 294, 1375–1385.
- Tenidis, K.; Waldner, M.; Bernhagen, J.; Fischle, W.; Bergmann, M.; Weber, M.; Merkle, M. L.; Voelter, W.; Brunner, H.; Kapurniotu, A. *J Mol Biol* 2000, 295, 1055–1071.
- Aziel, R.; Gazit, E. *J Biol Chem* 2001, 276, 34156–34161.
- Mazor, Y.; Gilead, S.; Benhar, I.; Gazit, E. *J Mol Biol* 2002, 322, 1013–1024.
- Jaikaran, E. T.; Higham, C. E.; Serpell, L. C.; Zurdo, J.; Gross, M.; Clark, A.; Fraser, P. E. *J. Mol Biol* 2001, 308, 515–525.
- Scrocchi, L. A.; Ha, K.; Chen, Y.; Wu, L.; Wang, F.; Fraser, P. E. *J Struct Biol* 2003, 141, 218–227.
- Laghaei, R.; Mousseau, N.; Wei, G. *J Phys Chem B* 2011, 115, 3146–3154.
- Tsolis, A. C.; Papandreou, N. C.; Iconomidou, V. A.; Hamodrakas, S. J. *PLoS ONE* 2013, 8, e54175.
- Liu, G.; Prabhakar, A.; Aucoin, D.; Simon, M.; Sparks, S.; Robbins, K. J.; Sheen, A.; Petty, S. A.; Lazo, N. D. *J Am Chem Soc* 2010, 132, 18223–18232.
- Wiltzius, J. J.; Sievers, S. A.; Sawaya, M. R.; Eisenberg, D. *Protein Sci* 2009, 18, 1521–1530.
- Mao, X. B.; Wang, C. X.; Wu, X. K.; Ma, X. J.; Liu, L.; Zhang, L.; Niu, L.; Guo, Y. Y.; Li, D. H.; Yang, Y. L.; Wang, C. *Proc Natl Acad Sci USA* 2011, 108, 19605–19610.

36. Barlos, K.; Gatos, D.; Kallitsis, J.; Papaphotiou, G.; Sotiriou, P.; Wenqing, Y.; Schäfer, W. *Tetrahedron Lett* 1989, 30, 3943–3946.
37. Louros, N. N.; Iconomidou, V. A.; Giannelou, P.; Hamodrakas, S. J. *PLoS ONE* 2013, 8, e73258.
38. Louros, N. N.; Iconomidou, V. A.; Tsiolaki, P. L.; Chrysina, E. D.; Baltatzis, G. E.; Patsouris, E. S.; Hamodrakas, S. J. *FEBS Lett* 2013, 588, 52–57.
39. Louros, N. N.; Petronikou, N.; Karamanos, T.; Cordopatis, P.; Iconomidou, V. A.; Hamodrakas, S. J. *Biopolymers* 2014, 102, 427–436.
40. Iconomidou, V. A.; Pheida, D.; Hamodraka, E. S.; Antony, C.; Hoenger, A.; Hamodrakas, S. J. *Biopolymers* 2011, 98, 67–75.
41. Romhanyi, G. *Virchows Arch A Pathol Anat Histopathol* 1971, 354, 209–222.
42. Oxford Diffraction. Chrysalis Promotions; In: *Diffraction*, Ed.; Oxford Diffraction Ltd.: Abingdon, Oxfordshire, England, 2009.
43. Leslie, A. G. W.; Powell, H. R., 2007. *Processing Diffraction Data with Mosflm*; (In: Read, R.; Sussman, J. L., Eds.; p. 41–51), *Evolving Methods for Macromolecular Crystallography*; Springer, Dordrecht, Vol. 245, pp. 41–51.
44. Savitsky, A.; Golay, M. J. E. *Anal Chem* 1964, 36, 1627–1639.
45. Tomasello, M. F.; Sinopoli, A.; Attanasio, F.; Giuffrida, M. L.; Campagna, T.; Milardi, D.; Pappalardo, G. *Eur J Med Chem* 2014, 81, 442–455.
46. Zhang, X.; Cheng, B.; Gong, H.; Li, C.; Chen, H.; Zheng, L.; Huang, K. *FEBS Lett* 2011, 585, 71–77.
47. Andrews, M. E.; Inayathullah, N. M.; Jayakumar, R.; Malar, E. J. *J Struct Biol* 2009, 166, 116–125.
48. Mezzenga, R.; Fischer, P. *Rep Prog Phys* 2013, 76, 046601.
49. Cai, S.; Singh, B. R. *Biophys Chem* 1999, 80, 7–20.
50. Haris, P. I.; Chapman, D. *Biopolymers* 1995, 37, 251–263.
51. Krimm, S.; Bandekar, J. *Adv Protein Chem* 1986, 38, 181–364.
52. Kong, J.; Yu, S. *Acta Biochim Biophys Sin (Shanghai)* 2007, 39, 549–559.
53. Jackson, M.; Mantsch, H. H. *Crit. Rev Biochem Mol Biol* 1995, 30, 95–120.
54. Divry, D.; Florkin, M. *Comptes Rendus de la Societe de Biologie* 1927, 97, 1808–1810.
55. Hamodrakas, S. J.; Hoenger, A.; Iconomidou, V. A. *J Struct Biol* 2004, 145, 226–235.
56. Iconomidou, V. A.; Leontis, A.; Hoenger, A.; Hamodrakas, S. J. *FEBS Lett* 2013, 587, 569–574.
57. Janciauskiene, S.; Ahren, B. *Biochem Biophys Res Commun* 1998, 251, 888–893.
58. Janson, J.; Ashley, R. H.; Harrison, D.; McIntyre, S.; Butler, P. C. *Diabetes* 1999, 48, 491–498.
59. Lorenzo, A.; Razzaboni, B.; Weir, G. C.; Yankner, B. A. *Nature* 1994, 368, 756–760.
60. Goldsbury, C.; Kistler, J.; Aebi, U.; Arvinte, T.; Cooper, G. J. *J Mol Biol* 1999, 285, 33–39.
61. Kaye, R.; Bernhagen, J.; Greenfield, N.; Sweimeh, K.; Brunner, H.; Voelter, W.; Kapurniotu, A. *J Mol Biol* 1999, 287, 781–796.
62. Goldsbury, C.; Goldie, K.; Pellaud, J.; Seelig, J.; Frey, P.; Muller, S. A.; Kistler, J.; Cooper, G. J.; Aebi, U. *J Struct Biol* 2000, 130, 352–362.
63. Exley, C.; House, E.; Patel, T.; Wu, L.; Fraser, P. E. *J Inorg Biochem* 2010, 104, 1125–1129.
64. Luca, S.; Yau, W. M.; Leapman, R.; Tycko, R. *Biochemistry* 2007, 46, 13505–13522.
65. Shim, S. H.; Gupta, R.; Ling, Y. L.; Strasfeld, D. B.; Raleigh, D. P.; Zanni, M. T. *Proc Natl Acad Sci USA* 2009, 106, 6614–6619.
66. Abedini, A.; Raleigh, D. P. *Protein Eng Des Sel* 2009, 22, 453–459.
67. Abedini, A.; Raleigh, D. P. *Phys Biol* 2009, 6, 015005.
68. Mishra, R.; Geyer, M.; Winter, R. *Chembiochem* 2009, 10, 1769–1772.
69. Brender, J. R.; Salamekh, S.; Ramamoorthy, A. *Acc Chem Res* 2011, 45, 454–462.
70. Patel, H. R.; Pithadia, A. S.; Brender, J. R.; Fierke, C. A.; Ramamoorthy, A. *J Phys Chem Lett* 2015, 5, 1864–1870.
71. Suzuki, Y.; Brender, J. R.; Hartman, K.; Ramamoorthy, A.; Marsh, E. N. *Biochemistry* 2012, 51, 8154–8162.
72. Soong, R.; Brender, J. R.; Macdonald, P. M.; Ramamoorthy, A. *J Am Chem Soc* 2009, 131, 7079–7085.
73. Sciacca, M. F.; Brender, J. R.; Lee, D. K.; Ramamoorthy, A. *Biochemistry* 2012, 51, 7676–7684.
74. Brender, J. R.; Hartman, K.; Nanga, R. P.; Popovych, N.; de la Salud Bea, R.; Vivekanandan, S.; Marsh, E. N.; Ramamoorthy, A. *J Am Chem Soc* 2010, 132, 8973–8983.
75. Brender, J. R.; Krishnamoorthy, J.; Messina, G. M.; Deb, A.; Vivekanandan, S.; La Rosa, C.; Penner-Hahn, J. E.; Ramamoorthy, A. *Chem Commun (Camb)* 2013, 49, 3339–3341.
76. Sciacca, M. F.; Milardi, D.; Messina, G. M.; Marletta, G.; Brender, J. R.; Ramamoorthy, A.; La Rosa, C. *Biophys J* 2013, 104, 173–184.
77. Brender, J. R.; Lee, E. L.; Hartman, K.; Wong, P. T.; Ramamoorthy, A.; Steel, D. G.; Gafni, A. *Biophys J* 2011, 100, 685–692.
78. Brender, J. R.; Heyl, D. L.; Samisetti, S.; Kotler, S. A.; Osborne, J. M.; Pesaru, R. R.; Ramamoorthy, A. *Phys Chem Chem Phys* 2013, 15, 8908–8915.
79. Brender, J. R.; Durr, U. H.; Heyl, D.; Budarapu, M. B.; Ramamoorthy, A. *Biochim Biophys Acta* 2007, 1768, 2026–2029.
80. Brender, J. R.; Lee, E. L.; Cavitt, M. A.; Gafni, A.; Steel, D. G.; Ramamoorthy, A. *J Am Chem Soc* 2008, 130, 6424–6429.
81. Brender, J. R.; Hartman, K.; Reid, K. R.; Kennedy, R. T.; Ramamoorthy, A. *Biochemistry* 2008, 47, 12680–12688.
82. Nanga, R. P.; Brender, J. R.; Xu, J.; Veglia, G.; Ramamoorthy, A. *Biochemistry* 2008, 47, 12689–12697.
83. Nanga, R. P.; Brender, J. R.; Vivekanandan, S.; Ramamoorthy, A. *Biochim Biophys Acta* 2011, 1808, 2337–2342.
84. Nanga, R. P.; Brender, J. R.; Xu, J.; Hartman, K.; Subramanian, V.; Ramamoorthy, A. *J Am Chem Soc* 2009, 131, 8252–8261.